*metals*

*Article*

# Application of Eh–pH Diagrams in the Hydrometallurgical Processing of Rare Earth Elements

**Ema Gánovská *, Martin Sisol, Martina Laubertová and Jakub Kurty**

Institute of Earth Resources, Faculty of Mining, Ecology, Process Control and Geotechnologies, Technical University of Košice, Letná 1/9, 042 00 Košice, Slovakia; martin.sisol@tuke.sk (M.S.); martina.laubertova@tuke.sk (M.L.); jakub.kurty@tuke.sk (J.K.)

* Correspondence: ema.ganovska@tuke.sk; Tel.: +421-55-602-2992

**Abstract**

Rare earth elements (REEs), including yttrium, scandium and lanthanides, are essential for advanced technologies, particularly in electronics, defense and renewable energy systems. The main primary REE sources include bastnaesite, monazite and ion-adsorption clays, while secondary sources comprise permanent magnets, phosphors, LEDs and other technological waste. The growing demand, together with China's dominant position in the global REE market and export restrictions, has increased concerns regarding the security of the REE supply in the European Union. This study evaluates selected primary REE resources and their processing possibilities using hydrometallurgical methods, with an emphasis on the thermodynamic aspects of REE leaching. The research focuses on the construction and analysis of Eh–pH diagrams generated using HSC Chemistry software to predict the stability of dissolved and solid species under different leaching conditions. These diagrams help identify suitable conditions for selective REE extraction and improve the understanding of the mechanisms governing hydrometallurgical processing. The results provide insight into the stability regions of REE species and indicate favorable conditions for selective leaching and recovery.

**Keywords:** rare earth elements; critical raw materials; hydrometallurgical processing; leaching; thermodynamics; Eh–pH diagrams

## 1. Introduction

REEs, including the fifteen lanthanides together with scandium and yttrium, represent a strategically important group of raw materials widely applied in modern technologies. Their unique physicochemical properties enable their application in permanent magnets, catalysts, rechargeable batteries, electronic devices, optical systems and advanced materials used in low-carbon and energy-efficient technologies [1,2]. In recent decades, global demand for REEs has increased considerably due to the rapid development of electromobility, renewable energy systems, automation and digital technologies. Despite their growing importance, the global REE supply chain remains highly concentrated, with most mining and processing capacities located in China [3]. This situation has increased concerns regarding supply security and strengthened the strategic importance of REEs for the European Union and other industrialized economies. In response to these challenges, the European Union has launched initiatives such as the Horizon Europe project SUPREEMO, aimed at strengthening European REE value chains and reducing dependence on China. Selected industrial applications of lanthanum, cerium and neodymium are summarized in Table 1.



Academic Editor: Corby G. Anderson

Received: 31 May 2026
Revised: 29 June 2026
Accepted: 1 July 2026
Published: 6 July 2026

**Table 1.** Selected industrial applications of REEs investigated in this study.

| Element | Industrial Sector | Representative Applications |
|---|---|---|
| Cerium (Ce) | Environmental technologies | Automotive catalytic converters, flue gas treatment |
| | Glass industry | Glass polishing powders, decolorizing agents, UV-resistant glass |
| | Energy technologies | Solid oxide fuel cells |
| Lanthanum (La) | Energy storage | Nickel-metal hydride batteries |
| | Chemical industry | Fluid catalytic cracking catalysts |
| | Optical industry | Optical glass, camera and telescope lenses |
| Neodymium (Nd) | Renewable energy | Wind turbine generators |
| | Electromobility | Electric vehicle motors |
| | Electronics | Hard disk drivers, speakers, consumer electronics |
| | Advanced manufacturing | Robotics and automation systems |

Although REEs are relatively abundant in the Earth's crust, economically exploitable concentrations occur only in specific geological environments and are commonly associated with complex mineralogical assemblages [4]. The most important primary REE resources are related mainly to carbonatites and alkaline igneous rocks, while ion-adsorption-clay deposits represent an important source of heavy REEs [5,6]. REEs are predominantly hosted in minerals such as bastnaesite, monazite and xenotime, whose chemical composition and structural characteristics strongly influence beneficiation and metallurgical processing behavior. In addition, many rare earth ores are characterized by fine-grained intergrowths with gangue minerals and may contain elevated concentrations of radioactive elements, which further complicates beneficiation and subsequent extraction processes [7,8].

Hydrometallurgical processing is widely used for the recovery of REEs from various raw materials due to its relatively high selectivity, lower energy consumption and suitability for the treatment of low-grade or compositionally complex ores. Among the available leaching systems, sulfuric acid and hydrochloric acid are commonly employed because of their ability to dissolve a broad range of REE-bearing phases. However, the dissolution behavior of REEs is strongly influenced by several physicochemical parameters, particularly pH, oxidation-reduction potential, temperature, and the stability of aqueous complexes formed during leaching [9]. Understanding the thermodynamic behavior under different leaching conditions is therefore essential for the optimization of hydrometallurgical processes and the improvement of selective extraction strategies [10].

Thermodynamic modeling, together with Eh–pH diagrams, provides an important basis for the evaluation of equilibrium conditions in aqueous systems. In hydrometallurgy, these diagrams are widely applied for the interpretation of leaching behavior, precipitation processes and the selective separation of metals from aqueous solutions. Their application is particularly important in REE systems, where aqueous chemistry is strongly influenced by complexation phenomena and changes in the oxidation state, especially in the case of cerium [10,11]. In recent years, thermodynamic software such as HSC Chemistry has become widely used for the construction and interpretation of Eh–pH diagrams, enabling equilibrium calculations in complex hydrometallurgical systems and supporting process design and optimization.

The present study is focused on the theoretical evaluation of cerium and lanthanum behavior in sulfuric acid and hydrochloric acid systems using Eh–pH diagrams. The work discusses the thermodynamic aspects of REE leaching with an emphasis on the stability of dissolved and solid species under different conditions of pH, oxidation-reduction potential and temperature. Attention is devoted to the interpretation of thermodynamic equilibria relevant to hydrometallurgical processing and the comparison of REE stability in chloride and sulfate media. The presented analysis aims to contribute to a better understanding of

the thermodynamic principles governing REE leaching systems and to provide a theoretical basis for the optimization of hydrometallurgical processing routes.

### *1.1. Primary Resources of REEs*

REEs occur in a wide range of geological environments and are associated with numerous mineral phases differing in chemical composition, physical properties and processability. The mineralogical composition of raw materials containing REEs strongly influences the selection of beneficiation and hydrometallurgical processing routes. Detailed mineralogical characterization is therefore essential for the design of efficient extraction and recovery processes [12].

Primary REE resources are predominantly associated with carbonatite deposits and alkaline igneous rocks. Carbonatites represent the most significant global source of REEs and account for a substantial proportion of their current industrial production. These deposits are typically enriched in light REEs and contain REE mineralization associated mainly with fluorocarbonates and phosphates, particularly bastnaesite, monazite, synchysite and parisite [13,14]. Besides these minerals, carbonatite ores commonly contain carbonate gangue minerals, iron oxides and hydroxides, which significantly affect beneficiation efficiency and subsequent leaching behavior [14]. Typical examples of carbonatite-related REE deposits include Bayan Obo in China, Mountain Pass in the USA and Mount Weld in Australia [15]. The global distribution of selected major REE deposits is shown in Figure 1.


**Figure 1.** Rare earth deposits. Data from Ref. [5].

Alkaline igneous rocks constitute another important source of REEs, particularly heavy REEs. In these deposits, REEs are commonly hosted in complex silicate minerals such as eudialyte, loparite and gadolinite. Compared with carbonatite ores, alkaline systems are generally characterized by more complicated mineralogical associations and finer intergrowths between valuable and gangue minerals [16].

In addition to conventional hard-rock deposits, ion-adsorption clay deposits represent an important source of heavy REEs. In these systems, REEs occur predominantly in an ion-exchangeable form adsorbed on the surface of clay minerals, which enables extraction under relatively mild leaching conditions without the need for intensive comminution or complex beneficiation operations [17].

Placer deposits enriched in monazite and xenotime also represent an important REE source; however, their processing is frequently complicated by the presence of radioactive elements such as thorium and uranium [5,6].

More than 250 minerals containing REEs have been identified, although only a limited number are considered economically significant. Their importance is mainly determined by

their REE content, abundance and occurrence in exploitable deposits [18]. Selected physical and chemical characteristics [19] of the important REE minerals are summarized in Table 2.

**Table 2.** Physical and chemical characteristics of principal REE minerals. Data from Ref. [19].

| Mineral | Formula | Color | Mohs Hardness | Density [kg/m$^3$] | Content of REO [1] [%] |
|---|---|---|---|---|---|
| Bastnaesite | (Ce, La, Nd, Pr)$CO_3F$ | Yellow, reddish brown, light green, brown | 4.0–4.5 | 4700–5100 | 65–75 |
| Monazite | (Ce, La, Nd, Pr, Th)$PO_4$ | Yellow-brown, brown, red, sometimes green | 5.05–5.5 | 4900–5500 | 55–70 |
| Xenotime | $YPO_4$ | Yellow, brown, sometimes yellowish green | 4.0–5.0 | 4400–5100 | 50–65 |
| Fergusonite | (Y, REE)$NbO_4$ | Yellow, tawny, black | 5.5–6.5 | 4900–5800 | 43–53 |
| Loparite | (Na, Ce, Ca, La, Sr)$O_3$(Ti, Nb) | Black, ash black, streak reddish brown | 5.6–6.0 | 4600–4900 | 30–40 |

[1] REO, Rare earth oxide.

The mineralogical composition and mode of REE occurrence significantly affect the behavior of rare earth elements during hydrometallurgical processing. The stability of minerals containing REEs, the presence of gangue phases and the occurrence of associated elements influence the selection of suitable leaching agents and process conditions [8]. Consequently, understanding the relationship between mineralogical characteristics and thermodynamic behavior is essential for the evaluation of REE leaching systems and the optimization of subsequent recovery processes.

### *1.2. Hydrometallurgical Processing of REEs from Primary Sources*

Hydrometallurgical processing is widely used for the extraction and recovery of REEs from both primary and alternative resources. Compared with pyrometallurgical methods, aqueous processing routes generally provide lower energy consumption, higher selectivity and better applicability to low-grade or compositionally complex ores. These processes are based on the dissolution of REE-bearing phases into aqueous solutions followed by the purification, separation and recovery of dissolved rare earth species. Process efficiency depends strongly on the mineralogical composition of the treated material, the stability of phases containing REEs and the physicochemical conditions during leaching [20,21].

#### 1.2.1. Leaching Agents and Conditions for REE Mineral Processing

The selection of a suitable leaching medium significantly affects the dissolution efficiency of REE minerals. Sulfuric acid and hydrochloric acid are among the most frequently used inorganic acids due to their high leaching efficiency and applicability to various ores that contain REEs. However, the behavior of individual minerals differs considerably depending on their chemical composition and the stability of reaction products formed during leaching [9]. Selected leaching agents commonly used for individual REE minerals are summarized in Table 3.

**Table 3.** Common leaching agents used for selected REE minerals. Data from Ref. [19].

| Mineral | Leaching Agents |
|---|---|
| Bastnaesite | HCl, $H_2SO_4$, $HNO_3$, $H_3PO_4$ |
| Monazite | $H_3PO_4$, $H_2SO_4$, $HClO_4$ |
| Fergusonite | Partially in HCl and fully in $H_2SO_4$, $H_3PO_4$, HF |
| Loparite | HF |

In addition to the type of leaching reagent, process performance is influenced by several operational parameters, including temperature, liquid-to-solid ratio, leaching time

and agitation conditions. Representative experimental studies reporting leaching conditions for selected primary and secondary REE resources are summarized in Table 4.

**Table 4.** Experimental leaching conditions reported for selected REE-bearing materials.

| Reference | Material | Quantitative Analysis | Leaching | |
|---|---|---|---|---|
| | | | Optimal Leaching Medium | Optimal Conditions |
| [22] | Bastnaesite concentrate | 65% REO [1] | 3 M HCl | T = 90 °C, L/S 9 mL/g, stirring at 300 rpm, t = 60 min |
| [23] | Monazite concentrate | 55–60% REO | Concentrated $H_2SO_4$ | Pretreatment—baking at 200–250 °C, leaching at atmospheric pressure, t = 2 h |
| [24] | Phosphogypsum ore | 0.1–0.3% REO | 2.5 M HCl | T = 45 °C, L/S = 29.8 mL/g, stirring at 300 rpm, t = 120 min |
| [25] | Bastnaesite concentrate (after non-oxidative roasting) | 68.72% REO | 3 M HCl (ultrasound-assisted) | T = 55 °C, ultrasound at 20 kHz, L/S = 10 mL/g, t = 60 min, stirring at 500 rpm |
| [26] | Ion-adsorption clays | 0.05–0.5% REO | 0.5 M $(NH_4)_2SO_4$ | pH 3–4, T = 50 °C, t = 5 min stirring at 900 rpm |
| [27] | Apatite ore | 3.07% La, 6.56% Ce, 0.54% Pr, 2.20% Nd, 0.22% Sm, 0.04% Eu, 0.07% Gd, 0.04% Dy, 0.02% Er, 0.27% Y | 1 M $H_2SO_4$ | T = 20 °C, t = 60 min, stirring at 500 rpm |

[1] REO, Rare earth oxide.

#### 1.2.2. Hydrometallurgical Processing of Bastnaesite

Hydrometallurgical processing of bastnaesite typically involves thermal treatment to decompose the fluorocarbonate structure and enhance subsequent REE extraction. Several roasting and leaching routes have been developed, with oxidation roasting followed by HCl leaching and sulfuric acid baking representing the most widely applied industrial technologies [28,29].

Oxidation roasting promotes the decomposition of bastnaesite and the oxidation of $Ce^{3+}$ to $Ce^{4+}$, resulting in the formation of acid-insoluble $CeO_2$. This phenomenon is advantageous because cerium remains in the solid residue, while most trivalent REEs can be selectively dissolved during subsequent hydrochloric acid leaching [30].

The oxidation roasting–HCl leaching–caustic conversion route was developed and industrially implemented by Molycorp [29].

Kruesi and Duker developed a three-stage processing route in which hydrochloric acid was used to dissolve rare earth carbonates according to Equation (1). The remaining fluoride phases were subsequently converted into hydroxides by reaction with sodium hydroxide according to Equation (2), while the resulting hydroxides were re-leached in hydrochloric acid to produce rare earth chloride solutions according to Equation (3) [9,31].

$$REF_3 - RE_2(CO_3)_3 + 9HCl = REF_3 + 2RECl_3 + 3HCl + 3H_2O + 3CO_2 \quad (1)$$

$$REF_3 + 3NaOH = RE(OH)_3 + 3NaF \quad (2)$$

$$RE(OH)_3 + 3HCl = RECl_3 + 3H_2O \quad (3)$$

The kinetics of hydrochloric acid leaching have been investigated by several authors. Zhang et al. (2017) studied the HCl leaching of Baotou bastnaesite and observed that increasing the acid concentration significantly improved REE extraction due to the higher availability of hydrogen ions promoting mineral dissolution [32]. Bian et al. (2011) reported that a thermal treatment at 400 °C for 3 h followed by HCl leaching enabled approximately 94.6% dissolution of carbonate phases while limiting fluoride dissolution to only 0.07% [33].

An alternative industrial route is sulfuric acid baking, which is currently employed for processing Bayan Obo concentrates. During this process, bastnaesite is treated with concentrated sulfuric acid at temperatures of 400–500 °C, converting REEs into soluble sulfates while releasing $CO_2$ and HF [31]. Feng et al. (2013) investigated the kinetics of sulfuric acid leaching of roasted Dechang bastnaesite from Sichuan, China, and reported that REE extraction was strongly influenced by the sulfuric acid concentration, temperature and particle size. Kinetic analysis indicated that the leaching process was controlled predominantly by diffusion through the product layer [34].

Similarly, Kul et al. (2008) achieved approximately 90% REE recovery from Turkish bastnaesite using sulfuric acid baking followed by water leaching [35]. Yörükoğlu et al. (2003) further demonstrated that the addition of thiourea prevented the oxidation of $Ce^{3+}$ during roasting and enabled its subsequent leaching together with other REEs [36].

Considerable research has focused on reducing fluorine emissions generated during conventional roasting. Chi et al. (2004) proposed ammonium chloride roasting, in which the thermal decomposition of $NH_4Cl$ generates HCl that reacts with rare earth oxides to form soluble rare earth chlorides. The authors also introduced fluorine deactivation by MgO addition prior to chlorination roasting, resulting in improved REE recovery and higher product purity [37]. Cen et al. (2016) developed a calcification roasting process based on $Ca(OH)_2$ addition, which converts fluorine into stable $CaF_2$, thereby reducing fluorine emissions and allowing its recovery as fluorite [38].

Several alternative activation and roasting techniques have been investigated for bastnaesite processing. Zhang and Saito (1998) investigated the mechanochemical activation of bastnaesite by milling with NaOH followed by hydrochloric acid leaching and reported REE extraction efficiencies approaching 90% [39]. Additional approaches including sodium carbonate roasting, calcium-based roasting for fluorine fixation, ammonium chloride roasting with fluorine deactivation, and aluminum hydroxide roasting have been proposed to improve fluorine fixation and simplify downstream hydrometallurgical treatment [37,40].

Although numerous alternative technologies have been proposed, oxidation roasting combined with HCl leaching and sulfuric acid baking remain the dominant industrial routes. Current research is focused primarily on increasing REE recovery, improving cerium management and minimizing fluorine emissions associated with bastnaesite processing.

#### 1.2.3. Hydrometallurgical Processing of Monazite

Hydrometallurgical processing of monazite has been extensively investigated in numerous experimental studies focused on mineral decomposition, leaching behavior and the selective recovery of REEs. The highly stable phosphate structure of monazite requires a preliminary decomposition step, which is generally achieved using either concentrated sulfuric acid or an alkaline sodium hydroxide treatment [23,41]. During the sulfuric acid digestion, rare earth phosphates are converted into soluble rare earth sulfates according to

Equation (4), while thorium phosphate is transformed into thorium sulfate as described by Equation (5) [23].

$$2REPO_4 + 3H_2SO_4 = RE_2(SO_4)_3 + 2H_3PO_4 \quad (4)$$

$$Th_3(PO_4)_4 + 6H_2SO_4 = 3Th(SO_4)_2 + 4H_3PO_4 \quad (5)$$

Subsequent water leaching enables the dissolution of the formed sulfates and the transfer of REEs into the solution [23]. Sadri et al. (2017) optimized the sulfuric acid digestion of Iranian monazite concentrate and reported recoveries of 92.34% Ce, 91.44% La and 92.10% Nd under conditions of 225 °C, 3.5 h and L/S ratio of 2.5. During the subsequent water leaching stage, recoveries of 88.47%, 89.45% and 87.35% were obtained for Ce, La and Nd, respectively [42].

Sulfuric acid baking has also been extensively studied by Demol et al. (2018), who investigated the phase transformations occurring during the thermal treatment of monazite concentrates between 200 and 800 °C. Their results showed that the sulfation of monazite was nearly complete after baking at 250 °C for 2 h, resulting in more than 90% dissolution of REEs, thorium and phosphate during subsequent leaching. Increasing the baking temperature to approximately 300 °C promoted the formation of thorium phosphate phases, which significantly reduced thorium solubility while maintaining almost complete extraction of REEs [23].

In addition to acidic processing routes, the alkaline decomposition using sodium hydroxide remains one of the most widely applied technologies for monazite treatment. During the alkaline digestion, rare earth phosphates are converted into rare earth hydroxides and trisodium phosphate according to Equation (6), while thorium phosphate undergoes a similar reaction to form thorium hydroxide and trisodium phosphate as described by Equation (7) [20,31].

$$REPO_4 + 3NaOH = RE(OH)_3 + Na_3PO_4 \quad (6)$$

$$Th_3(PO_4)_4 + 12NaOH = 3Th(OH)_4 + 4Na_3PO_4 \quad (7)$$

The trisodium phosphate produced during the alkaline decomposition can be recovered as a valuable by-product, whereas the hydroxide residue containing rare earth and thorium hydroxides is subsequently dissolved in acidic media. Hydrochloric acid is commonly employed to convert rare earth hydroxides into soluble chloride species according to Equation (8), while thorium hydroxide is dissolved to form thorium chloride as described by Equation (9) [20,29].

$$RE(OH)_3 + 3HCl = RECl_3 + 3H_2O \quad (8)$$

$$Th(OH)_4 + 4HCl = ThCl_4 + 4H_2O \quad (9)$$

Panda et al. (2014) investigated the alkaline decomposition of a Korean monazite concentrate using 50 wt.% NaOH and reported approximately 95% REE recovery under optimized conditions at 170 °C [41].

Alternative decomposition technologies have been proposed to overcome some of the limitations of conventional acid and alkaline routes. One such process involves high-temperature treatment of monazite with $CaCl_2$ and $CaCO_3$ under reducing and sulfidizing conditions, resulting in the formation of rare earth oxysulfides and oxychlorides that can subsequently be leached using dilute hydrochloric acid [20,31]. Compared with conventional alkaline digestion, this approach offers shorter reaction times and eliminates the need for fine grinding. However, the overall REE recovery remains lower than that achieved by alkaline processing, which has limited its industrial application [31].

Recent reviews indicate that sulfuric acid baking and alkaline cracking remain the dominant industrial approaches for monazite processing, while current research is focused mainly on improving REE recovery, reducing thorium mobility, and optimizing the selectivity of subsequent hydrometallurgical separation stages [20,43].

#### 1.2.4. Hydrometallurgical Processing of Ion-Adsorption Clays

Unlike conventional hard-rock REE deposits, ion-adsorption clays can be processed without intensive comminution, beneficiation or mineral decomposition. The recovery of REEs is based primarily on ion-exchange reactions, during which adsorbed rare earth ions are displaced from the surface of clay minerals by competing cations present in the leaching solution [26,44].

A variety of leaching agents has been evaluated for this purpose, including ammonium sulfate, ammonium chloride, ammonium nitrate and sodium chloride solutions. Among them, ammonium sulfate remains the most widely applied reagent in industrial practice due to its favorable extraction efficiency and relatively low operating costs. During leaching, ammonium ions replace adsorbed rare earth ions on the surface of clay minerals through an ion-exchange mechanism according to Equation (10) [20,31].

$$[Al_2Si_2O_5(OH)_4] \cdot RE^{3+} + 3NH_4^+ = [Al_2Si_2O_5(OH)_4] \cdot (NH_4^+)_3 + RE^{3+} \quad (10)$$

The leaching process is characterized by rapid kinetics, with the equilibrium commonly reached within a few minutes. Moldoveanu and Papangelakis (2013) reported REE extraction efficiencies of 80–90% using ammonium sulfate solutions. Commercial operations in China achieve recoveries of up to 95% from ion-adsorption clays using low-concentration ammonium sulfate (1–2 wt.%) or sodium chloride solutions (~7 wt.%) at pH values close to 4 [31,45].

Recent studies have investigated magnesium sulfate as an alternative leaching reagent for ion-adsorption clays. Comparable REE extraction efficiencies to those obtained with ammonium sulfate were reported, while the environmental impacts associated with ammonia–nitrogen contamination were significantly reduced [46,47].

Industrial processing of ion-adsorption clays has evolved from pool and heap leaching to the currently dominant in situ leaching technology, which minimizes ore handling and reduces operating costs. After leaching, impurity elements such as Al, Fe and Ca are removed by neutralization, while REEs are subsequently recovered by precipitation or solvent extraction prior to further purification and separation [8].

#### 1.2.5. Thermodynamic Evaluation Using Eh–pH Diagrams

Thermodynamic analysis represents an important part of hydrometallurgical process evaluation, particularly in systems where dissolved and precipitated species are strongly affected by physicochemical conditions [48]. In aqueous rare earth systems, parameters such as pH, oxidation-reduction potential, and temperature significantly influence the distribution of individual chemical species. For this reason, thermodynamic modeling is commonly applied for the prediction of phase stability and the interpretation of the dissolution and precipitation processes occurring during hydrometallurgical treatment [10].

Eh–pH diagrams describe the thermodynamic stability regions of dissolved and precipitated species in aqueous systems as a function of pH and electrode potential. Their construction is based on equilibrium calculations derived from Gibbs free energy data and electrochemical relationships. Gibbs free energy may be expressed according to Equation (11).

$$\Delta G = \Delta H - T\Delta S \quad (11)$$

where ΔG is the Gibbs free energy change, ΔH is the enthalpy change, T is the thermodynamic temperature, and ΔS is the entropy change [49].

In thermodynamic studies, the Gibbs free energy serves as an important criterion for assessing the feasibility of chemical reactions. Negative values of ΔG indicate spontaneous processes, whereas positive values indicate reactions that are thermodynamically unfavorable under the specified conditions [49].

In hydrometallurgy, Eh–pH diagrams provide useful information regarding the conditions under which the dissolution, hydrolysis, oxidation or precipitation of metallic species may occur. Stability boundaries correspond to equilibrium conditions between dissolved and solid phases or between species differing in the oxidation state. The diagrams commonly include aqueous ions, hydroxides, oxides, sulfates and chloride complexes, depending on the composition of the investigated medium [48,49].

Most REEs occur predominantly in the trivalent oxidation state and therefore exhibit relatively similar behavior in aqueous systems. Cerium represents an exception due to the stability of both $Ce^{3+}$ and $Ce^{4+}$ species, which significantly affects its dissolution and precipitation behavior under oxidizing conditions [29]. This redox variability may play an important role during the selective separation and purification of cerium from other REEs [50].

The stability of REE species is strongly influenced by pH. Under acidic conditions, REEs generally remain stable in dissolved ionic or complexed forms, whereas increasing the pH promotes hydrolysis reactions and the precipitation of hydroxides or oxide phases. The oxidation-reduction potential additionally affects species with variable oxidation states, while the temperature may shift equilibrium boundaries and modify the extent of hydrolysis or complexation reactions [10].

Despite their considerable usefulness, Eh–pH diagrams exhibit certain limitations. The diagrams describe equilibrium conditions only and do not provide information regarding reaction kinetics, mass transfer limitations or metastable phase formation [48,49]. In real hydrometallurgical systems, equilibrium may not always be achieved due to slow dissolution rates, incomplete reactions or complex mineralogical associations [48]. Furthermore, the reliability of calculated stability regions depends strongly on the availability and accuracy of the thermodynamic data for the investigated species. Nevertheless, Eh–pH diagrams remain valuable tools for interpretation of aqueous REE systems and the evaluation of conditions relevant to hydrometallurgical leaching and separation processes [10,49].

The present study evaluates the thermodynamic stability and dissolution–precipitation behavior of cerium and lanthanum in chloride and sulfate media at temperatures up to 80 °C using Eh–pH diagrams. Particular attention is devoted to the comparative analysis of chloride and sulfate systems in order to assess the influence of sulfate complexation on the stability of dissolved species. Furthermore, the specific redox behavior of the $Ce^{3+}/Ce^{4+}$ system is examined with respect to its potential application in the selective separation of REEs.

Although Eh–pH diagrams have previously been used to investigate the thermodynamic behavior of rare earth elements in aqueous systems, most published studies focus on individual elements or specific leaching environments. The novelty of the present study lies in the comprehensive comparison of cerium, lanthanum, and neodymium in both chloride and sulfate media at temperatures relevant to hydrometallurgical processing, an approach that remains limited in the available literature. Furthermore, the application of such thermodynamic evaluations as a basis for the design of subsequent experimental leaching studies has received relatively little attention. Addressing these aspects may contribute to a better understanding of REE behavior under different processing conditions and support the optimization of hydrometallurgical recovery routes. Therefore, the aim of this study

was to evaluate the thermodynamic behavior of cerium, lanthanum and neodymium in chloride and sulfate systems at 25 °C and 80 °C using Eh–pH diagrams generated in HSC Chemistry software.

## 2. Methods

Thermodynamic evaluation of REE behavior in aqueous systems was performed using Pourbaix (Eh–pH) diagrams generated with the Eh–pH Diagrams module of the HSC Chemistry software (version 10.0.2.3, Metso Finland Oy, Espoo, Finland; University Basic License). The software calculates equilibrium stability fields of aqueous and solid species based on the thermodynamic data stored in the HSC database. Eh–pH diagrams were constructed for Ce–Cl–$H_2O$, La–Cl–$H_2O$, Ce-F-C-Cl-$H_2O$, Ce–S–$H_2O$, La–S–$H_2O$, Ce-F-C-S- $H_2O$ systems at 25 °C and 80 °C in order to evaluate the stability of dissolved ions, complexes and precipitated phases under different pH and redox conditions. The calculations were performed at a concentration of 1 mol·dm$^{-3}$ to ensure a consistent comparison between the investigated systems.

It should be noted that the reliability of Eh–pH diagrams depends on the availability and accuracy of the thermodynamic data used for equilibrium calculations. Although the HSC Chemistry database contains extensive thermodynamic information for a wide range of aqueous and solid species, some rare earth element species may have limited or less comprehensive thermodynamic datasets. Consequently, the calculated stability fields should be interpreted as thermodynamic predictions under equilibrium conditions and may not fully reflect the behavior of real hydrometallurgical systems. Therefore, experimental verification remains important for confirming the predicted stability regions and species distributions.

## 3. Results and Discussion

### *3.1. Thermodynamic Study of the Ce–Cl–$H_2O$ System*

Cerium exhibits more complex equilibrium behavior than most rare earth elements due to the stability of both trivalent and tetravalent oxidation states. In chloride systems, strongly acidic and reducing conditions favor the stabilization of dissolved $Ce^{3+}$ species, whereas increasing the oxidation-reduction potential promotes the oxidation of $Ce^{3+}$ to $Ce^{4+}$ followed by the stabilization of $CeO_2$. The calculated stability regions for the Ce–Cl–$H_2O$ system at 25 °C and 80 °C are presented in Figure 2.

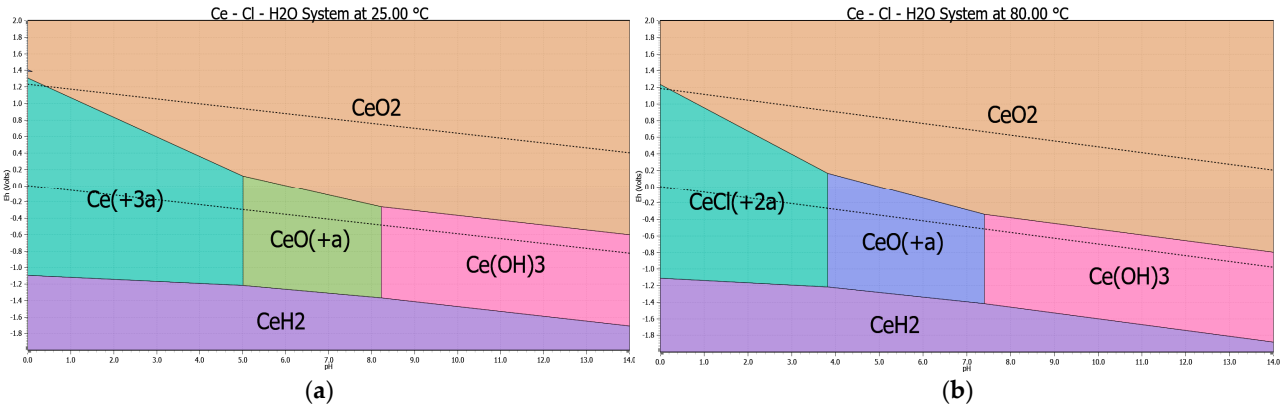


(**a**) (**b**)

**Figure 2.** Eh–pH diagrams for the leaching of Ce in HCl at temperatures of 25 °C and 80 °C: (**a**) The Ce-Cl-$H_2O$ system at temperature of 25 °C; (**b**) The Ce-Cl-$H_2O$ system at temperature of 80 °C. Note: The molalities of the elements are set at 1 mol·kg$^{-1}$ $H_2O$, with the upper and lower stability limits of $H_2O$ defined by the dashed lines.

Under highly acidic conditions, dissolved cerium species predominate over a relatively broad Eh range, indicating suitable thermodynamic conditions for hydrochloric acid leaching. With increasing pH, gradual hydrolysis occurs and the stability field shifts toward hydrolyzed $CeO^+$ species, followed by the precipitation of $Ce(OH)_3$ in alkaline environments. In oxidizing regions, $CeO_2$ remains stable over a wide pH interval, reflecting the strong tendency of cerium to form tetravalent oxide phases.

Compared with the diagram calculated at 25 °C, the system at 80 °C shows a noticeable displacement of equilibrium boundaries toward lower pH values. The onset of hydrolysis shifts from approximately pH 5.0 at 25 °C to pH 4.0 at 80 °C, while the transition from hydrolyzed $CeO^+$ species to $Ce(OH)_3$ precipitation occurs at approximately pH 8.2 and pH 7.5, respectively. In addition, the stability boundary separating dissolved cerium species from $CeO_2$ is shifted toward lower Eh values by approximately 0.2 V. These changes indicate that elevated temperature promotes hydrolysis reactions and modifies the stability fields of dissolved cerium species. Nevertheless, acidic chloride environments still maintain favorable conditions for the dissolution of cerium-bearing phases.

From a hydrometallurgical point of view, the stabilization of $CeO_2$ under oxidizing conditions may become technologically significant during downstream processing. The oxidative conversion of $Ce^{3+}$ to $Ce^{4+}$ can potentially be utilized during the selective separation of cerium from other trivalent rare earth elements because tetravalent cerium exhibits substantially different precipitation and complexation behavior.

### *3.2. Thermodynamic Study of the La–Cl–$H_2O$ System*

Unlike cerium, lanthanum remains stable exclusively in the trivalent oxidation state and therefore exhibits considerably simpler equilibrium behavior in chloride systems. The stability regions observed in the La–Cl–$H_2O$ diagrams are controlled predominantly by pH-dependent hydrolysis reactions rather than redox transformations. Figure 3 shows the calculated thermodynamic stability fields for the La–Cl–$H_2O$ system at 25 °C and 80 °C.

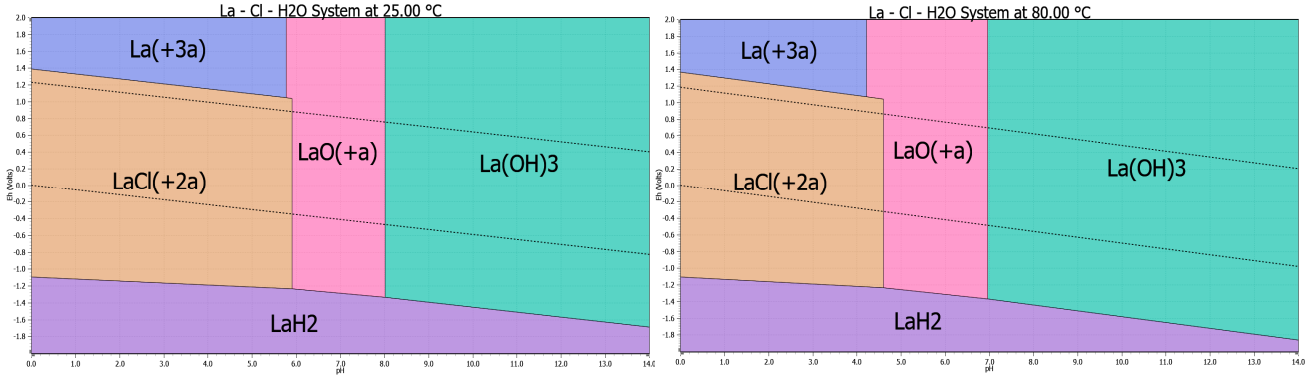


(**a**) (**b**)

**Figure 3.** Eh–pH diagrams of La leaching in HCl at temperatures of 25 °C and 80 °C: (**a**) The La-Cl-$H_2O$ system at temperature of 25 °C; (**b**) The La-Cl-$H_2O$ system at temperature of 80 °C. Note: The molalities of the elements are set at 1 mol·kg$^{-1}$ $H_2O$, with the upper and lower stability limits of $H_2O$ defined by the dashed lines.

In acidic chloride media, dissolved $La^{3+}$ ions and $LaCl^{2+}$ aqueous complexes remain stable within broad pH regions. Increasing the pH gradually promotes hydrolysis and the formation of intermediate $LaO^+$ species, followed by the precipitation of $La(OH)_3$ under alkaline conditions. Compared with cerium systems, the equilibrium boundaries are considerably simpler and exhibit only limited dependence on the oxidation-reduction potential.

An increase in temperature to 80 °C results in a noticeable expansion of the hydrolysis region and shifts the stability boundaries toward lower pH values. The transition from

dissolved lanthanum species to hydrolyzed $LaO^+$ species occurs at approximately pH 6.0 at 25 °C and pH 4.5 at 80 °C. Similarly, the onset of $La(OH)_3$ precipitation is shifted from approximately pH 8.0 to pH 7.0. These changes indicate that elevated temperature promotes hydrolysis and reduces the pH range over which dissolved lanthanum species remain stable. Nevertheless, the overall thermodynamic behavior remains relatively simple, and the predominance of dissolved lanthanum species under acidic conditions confirms the suitability of hydrochloric acid systems for the leaching of lanthanum-bearing minerals.

Despite the temperature-induced shifts in the hydrolysis boundaries, chloride systems remain characterized by relatively simple aqueous speciation. Compared with sulfate media, chloride systems exhibit less extensive aqueous complexation, which may simplify downstream purification and precipitation processes. More defined hydrolysis regions may therefore provide better control of the pH-dependent recovery operations during hydrometallurgical treatment.

### *3.3. Thermodynamic Study of the Nd–Cl–$H_2O$ System*

The equilibrium behavior of neodymium in hydrochloric acid solutions is governed predominantly by acid–base equilibria because neodymium remains thermodynamically stable only in the trivalent oxidation state. Consequently, unlike cerium, no redox-controlled phase transitions are observed within the investigated stability range. The calculated predominance diagrams for the Nd–Cl–$H_2O$ system at 25 °C and 80 °C are presented in Figure 4.

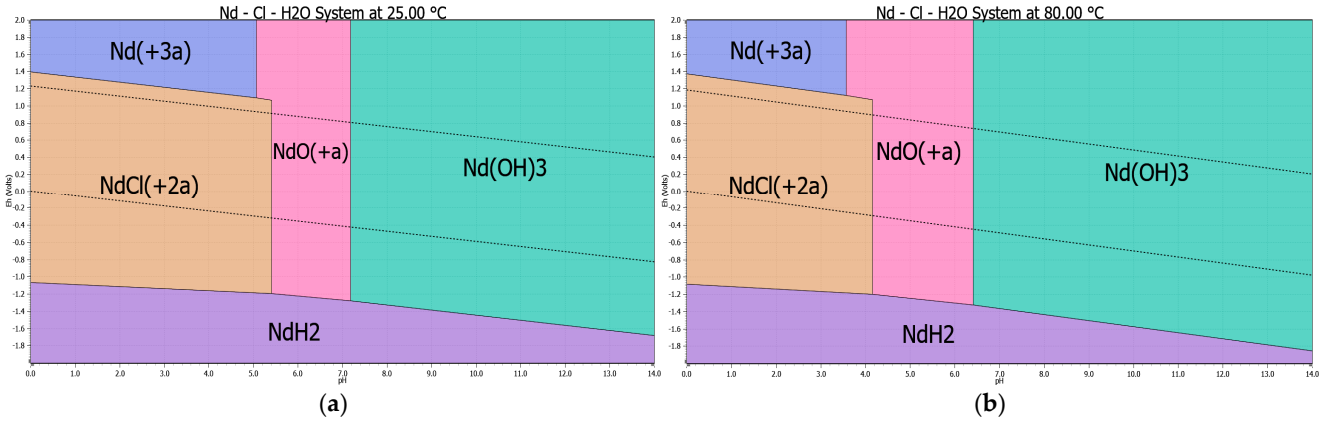


(**a**) (**b**)

**Figure 4.** Eh–pH diagrams of Nd leaching in HCl at temperatures of 25 °C and 80 °C: (**a**) The Nd-Cl-$H_2O$ system at temperature of 25 °C; (**b**) The Nd-Cl-$H_2O$ system at temperature of 80 °C. Note: The molalities of the elements are set at 1 mol·$kg^{-1}$ $H_2O$, with the upper and lower stability limits of $H_2O$ defined by the dashed lines.

Under strongly acidic conditions, dissolved $Nd^{3+}$ ions represent the predominant species, while the formation of aqueous chloride complexes ($NdCl^{2+}$) further extends the stability of dissolved neodymium in hydrochloric media. As the pH increases, hydrolysis becomes thermodynamically favorable, leading first to the appearance of the intermediate hydrolyzed species $NdO^+$ and subsequently to the precipitation of $Nd(OH)_3$ under near-neutral and alkaline conditions. The predominance fields exhibit only minor dependence on the oxidation-reduction potential, confirming that pH is the principal variable controlling neodymium speciation in chloride systems.

Increasing the temperature from 25 °C to 80 °C shifts the hydrolysis equilibria toward more acidic conditions. The boundary between dissolved $Nd^{3+}$ species and $NdO^+$ moves from approximately pH 5.0 to pH 4.0, while the transition from $NdO^+$ to solid $Nd(OH)_3$ shifts from approximately pH 7.2 at 25 °C to about pH 6.4 at 80 °C. At the same time, the stability field of the aqueous chloride complex $NdCl^{2+}$ becomes slightly broader at lower

pH values, indicating a modest increase in chloride complex stability with temperature. In contrast to cerium, no temperature-induced changes associated with oxidation state transitions are observed.

From a processing perspective, these results indicate that hydrochloric acid solutions provide favorable thermodynamic conditions for the dissolution of neodymium-bearing minerals over a relatively broad acidic pH range. However, the observed shift in hydrolysis boundaries toward lower pH values at elevated temperature suggests that pH control becomes increasingly important during high-temperature leaching to prevent the premature precipitation of $Nd(OH)_3$. The absence of competing tetravalent species further simplifies neodymium behavior in chloride media and facilitates subsequent separation from cerium, whose redox chemistry differs substantially under comparable leaching conditions.

### *3.4. Thermodynamic Study of Bastnaesite and Monazite Leaching in Hydrochloric Acid Media*

Bastnäsite and monazite represent the two principal primary rare earth minerals exploited for industrial REE production. Although both minerals serve as major sources of REEs, their chemical compositions differ substantially, resulting in different thermodynamic behavior during hydrometallurgical processing. Bastnäsite is a fluorocarbonate mineral, whereas monazite is a rare earth phosphate. Consequently, the dissolution of these minerals proceeds through different reaction pathways and may lead to the formation of different secondary phases. To evaluate the thermodynamic feasibility of representative dissolution reactions, the reactions described by Equations (12)–(17) were assessed by calculating the corresponding thermodynamic parameters. The calculated enthalpy (ΔH), entropy (ΔS), and Gibbs free energy (ΔG) values for the hydrochloric acid system are summarized in Table 5.

**Table 5.** Calculated thermodynamic parameters for representative dissolution reactions of bastnäsite and monazite in hydrochloric acid.

| Mineral | Chemical Reaction | T [°C] | ΔH [kJ] | ΔS [J/K] | ΔG [kJ] | No. |
|---|---|---|---|---|---|---|
| Bastnaesite | $Ce_2O_3 + 6HCl_{(ia)} = 2CeCl_{3(a)} + 3H_2O$ | 25 | −414.262 | −256.348 | −337.832 | (12) |
| | | 80 | −391.985 | −188.472 | −325.426 | |
| | $La_2O_3 + 6HCl_{(ia)} = 2LaCl_{3(a)} + 3H_2O$ | 25 | −459.330 | −284.259 | −374.578 | (13) |
| | | 80 | −432.700 | −202.926 | −361.036 | |
| | $CeO_2 + 4HCl_{(ia)} = CeCl_{4(a)} + 2H_2O$ | 25 | −18.988 | −217.142 | 45.753 | (14) |
| | | 80 | 11.883 | −122.301 | 55.074 | |
| Monazit | $CePO_4 + 3HCl_{(ia)} = CeCl_{3(a)} + H_3PO_{4(a)}$ | 25 | −46.924 | −116.757 | −12.113 | (15) |
| | | 80 | −37.199 | −87.206 | −6.402 | |
| | $LaPO_4 + 3HCl_{(ia)} = LaCl_{3(a)} + H_3PO_{4(a)}$ | 25 | −43.340 | −129.713 | −4.666 | (16) |
| | | 80 | −31.430 | −93.409 | 1.557 | |
| | $NdPO_4 + 3HCl_{(ia)} = NdCl_{3(a)} + H_3PO_{4(a)}$ | 25 | −37.059 | −126.501 | 0.657 | (17) |
| | | 80 | −33.711 | −116.667 | 7.490 | |

Note: "a" denotes an aqueous species, while "ia" denotes an aqueous species whose thermodynamic properties are calculated from its ionic components, according to the HSC Chemistry database notation.

Bastnaesite, commonly represented by the general formula $LnCO_3F$ (Ln = Ce, La), may generate fluoride-bearing species during acidic processing. Cerium occurs predominantly in the trivalent oxidation state $Ce^{3+}$, although oxidation to $Ce^{4+}$ may occur under oxidizing conditions, resulting in the formation of highly stable oxide phases. As shown in Figure 5, the stability of cerium species is strongly dependent on both pH and redox potential.

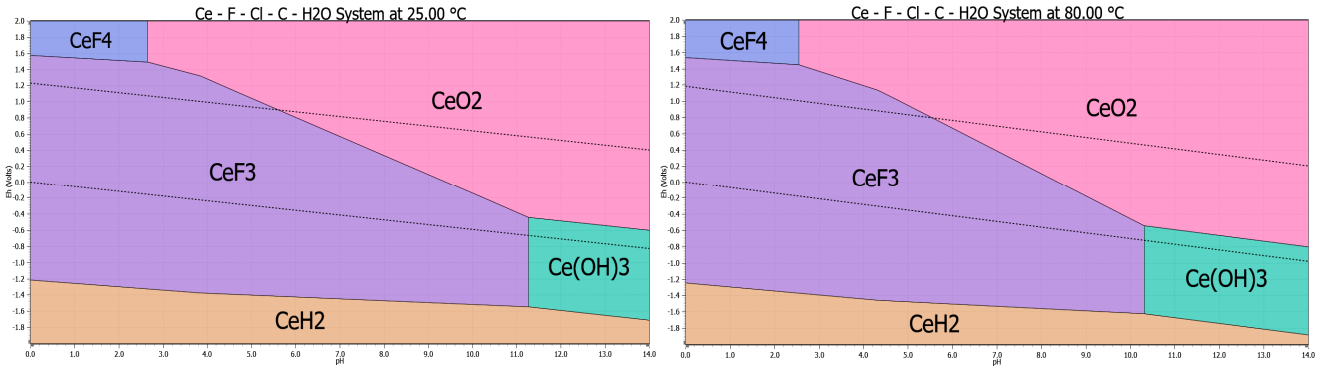


(**a**) (**b**)

**Figure 5.** Eh–pH diagrams of leaching bastnaesite in HCl at temperatures of 25 °C and 80 °C: (**a**) The Ce-F-C-Cl-$H_2O$ system at temperature of 25 °C; (**b**) The Ce-F-C-Cl-$H_2O$ system at temperature of 80 °C. Note: The molalities of the elements are set at 1 mol·kg$^{-1}$ $H_2O$, with the upper and lower stability limits of $H_2O$ defined by the dashed lines.

As summarized in Table 5, the calculated Gibbs free energy values are negative at both investigated temperatures, confirming that the dissolution of $Ce_2O_3$ in hydrochloric acid is thermodynamically spontaneous. Although the absolute value of ΔG decreases slightly with increasing the temperature, indicating a minor reduction in the thermodynamic driving force, the reaction remains highly favorable throughout the investigated temperature range.

The Eh–pH diagrams indicate that dissolved trivalent cerium species remain stable over a broad range of acidic conditions. At 25 °C, fluoride-bearing cerium species are thermodynamically stable under strongly acidic conditions within the stability region of water, particularly at pH values below approximately 4. Increasing the temperature to 80 °C causes only a slight displacement of the stability boundaries between dissolved and solid cerium species, while the overall distribution of cerium species remains nearly unchanged. The transition between dissolved $Ce^{3+}$ species and $CeO_2$ shifts only moderately, whereas $CeF_4$ remains stable under strongly acidic and oxidizing conditions. These observations indicate that temperature has only a limited influence on cerium speciation within the investigated range.

The extensive stability field of $CeO_2$ observed in Figure 5 confirms the exceptional thermodynamic stability of tetravalent cerium under oxidizing conditions. Consequently, the oxidation of $Ce^{3+}$ to $Ce^{4+}$ substantially decreases cerium solubility and may limit its recovery during hydrometallurgical processing. Industrial hydrometallurgical processing often employs reducing environments or reducing agents to convert $Ce^{4+}$ to the more soluble $Ce^{3+}$ form and thereby enhance cerium dissolution.

The positive Gibbs free energy values listed in Table 5 indicate that the dissolution of $CeO_2$ in hydrochloric acid is thermodynamically unfavorable and therefore does not occur spontaneously under the investigated conditions. Furthermore, the increase in ΔG with temperature suggests that elevated temperatures do not improve the thermodynamic feasibility of $CeO_2$ dissolution. This behavior is fully consistent with the large $CeO_2$ stability field observed in the Eh–pH diagrams.

Although $CeO_2$ is thermodynamically stable under oxidizing conditions, industrial hydrometallurgical processing commonly employs reducing environments or suitable reducing agents to convert $Ce^{4+}$ into the considerably more soluble $Ce^{3+}$ form, thereby enhancing cerium dissolution.

In addition to cerium oxide formation, the fluoride released from bastnäsite during acidic decomposition may promote the precipitation of fluoride-bearing cerium compounds, particularly under strongly acidic conditions. The formation of these secondary phases

may decrease the concentration of dissolved cerium species and consequently influence the overall leaching efficiency.

Figure 6 illustrates the variation in the Gibbs free energy with temperature for the representative dissolution reactions of $Ce_2O_3$, $La_2O_3$ and $CeO_2$ in hydrochloric acid. The figure provides a direct comparison of the thermodynamic behavior of trivalent and tetravalent rare earth oxides over a broad temperature range.

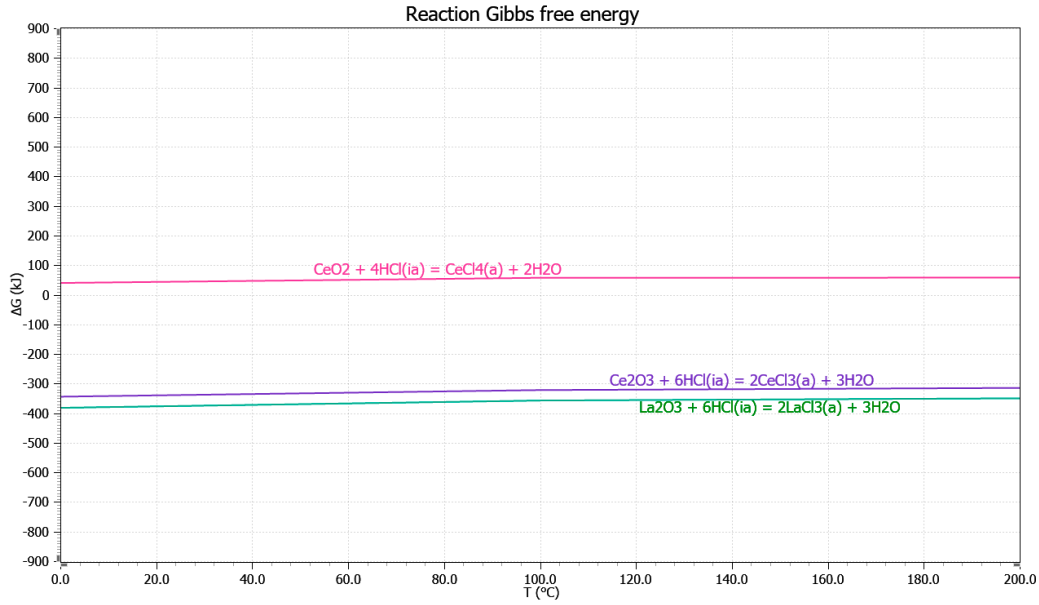


**Figure 6.** Graph of dependence of ΔG values of Equations (12)–(14) on temperature. Note: "a" denotes an aqueous species, while "ia" denotes an ion-associated aqueous species according to the HSC Chemistry database notation.

As shown in Figure 6, the dissolution of $Ce_2O_3$ and $La_2O_3$ is characterized by consistently negative Gibbs free energy values throughout the investigated temperature interval, confirming that both reactions remain thermodynamically spontaneous. Although the absolute values of ΔG gradually decrease with increasing the temperature, only a minor reduction in the thermodynamic driving force is observed. In contrast, the dissolution of $CeO_2$ exhibits positive Gibbs free energy values over the entire temperature range, which increase slightly with temperature, further confirming the exceptional stability of tetravalent cerium oxide.

Overall, the thermodynamic analysis demonstrates that hydrochloric acid readily dissolves trivalent rare earth oxides associated with bastnäsite, whereas $CeO_2$ remains highly resistant to dissolution under oxidizing conditions. Consequently, maintaining reducing conditions during leaching is essential for maximizing cerium recovery from bastnäsite concentrates.

Unlike bastnäsite, monazite is a phosphate mineral in which rare earth elements are incorporated into a highly stable phosphate lattice. The strong REE–phosphate bonds make monazite considerably more resistant to acidic dissolution than fluorocarbonate minerals. Although hydrochloric acid is not the conventional reagent for industrial monazite processing, the evaluation of its thermodynamic behavior in chloride media enables a direct comparison with bastnäsite under identical chemical conditions.

Figure 7 illustrates the temperature dependence of the Gibbs free energy of the representative dissolution reactions of rare earth phosphates in hydrochloric acid. The figure demonstrates the influence of temperature on the thermodynamic feasibility of monazite decomposition and enables a direct comparison of the stability of the investigated phosphate phases.

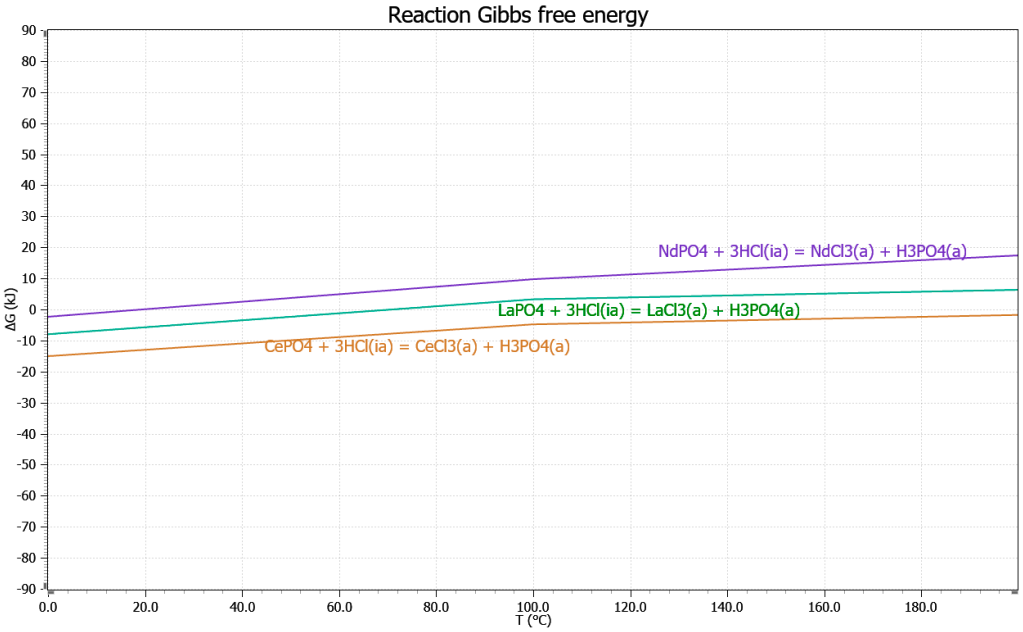


**Figure 7.** Graph of dependence of ΔG values of Equations (15)–(17) on temperature. Note: "a" denotes an aqueous species, while "ia" denotes an ion-associated aqueous species according to the HSC Chemistry database notation.

Although the calculated Gibbs free energy values decrease substantially with increasing the temperature, negative values are reached only at temperatures considerably higher than those typically employed in conventional hydrometallurgical leaching. Therefore, the results indicate that temperature alone is insufficient to achieve spontaneous monazite decomposition under practical processing conditions. Efficient dissolution of monazite generally requires more aggressive operating conditions, prolonged leaching times, or highly concentrated acidic media to overcome the exceptional stability of the phosphate lattice.

Comparison of the thermodynamic behavior of bastnäsite and monazite demonstrates that the two minerals exhibit fundamentally different dissolution characteristics in hydrochloric acid. Whereas the dissolution of bastnäsite-derived rare earth oxides is characterized by negative Gibbs free energy values and, therefore, proceeds spontaneously under acidic conditions, rare earth phosphates derived from monazite remain significantly more stable. This difference originates primarily from the high thermodynamic stability of the REE–phosphate bonds in the monazite crystal structure. Consequently, the mineralogical composition plays a decisive role in determining the suitability of hydrochloric acid as a leaching agent and should be carefully considered when designing hydrometallurgical processing routes for primary rare earth ores.

### *3.5. Thermodynamic Study of the Ce–S–$H_2O$ System*

The thermodynamic behavior of cerium in sulfate systems differs substantially from that observed in chloride media due to the strong sulfate complexation effects. In sulfuric acid environments, dissolved cerium species remain stable over broad acidic regions, while the sulfate-containing aqueous complexes significantly modify the equilibrium relationships between the dissolved and precipitated phases. The corresponding Ce–S–$H_2O$ diagrams calculated at 25 °C and 80 °C are shown in Figure 8.

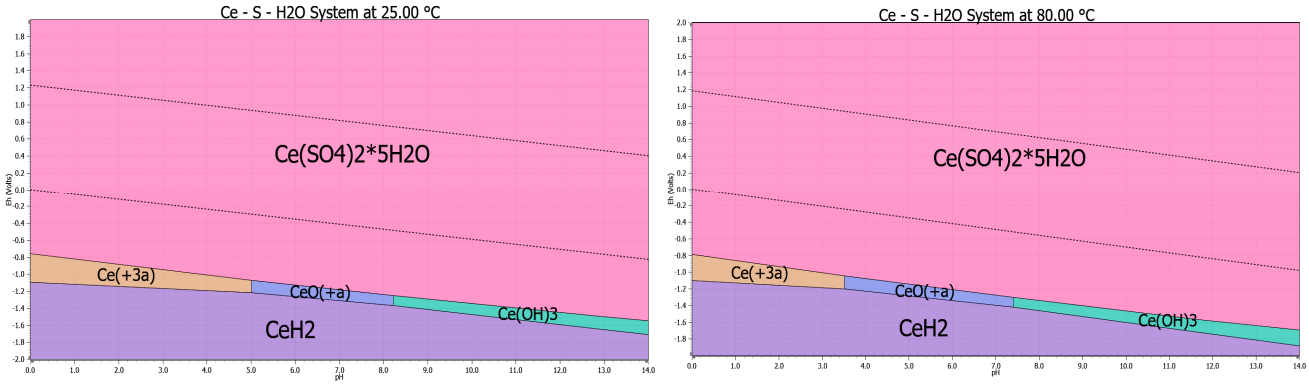


(**a**) (**b**)

**Figure 8.** Eh–pH diagrams of Ce leaching in $H_2SO_4$ at temperatures of 25 °C and 80 °C: (**a**) The Ce-S-$H_2O$ system at temperature of 25 °C; (**b**) The Ce-S-$H_2O$ system at temperature of 80 °C. Note: The molalities of the elements are set at 1 mol·kg$^{-1}$ $H_2O$, with the upper and lower stability limits of $H_2O$ defined by the dashed lines.

The stabilization of dissolved cerium species in sulfate media is associated with the formation of sulfate complexes. The corresponding complexation reactions may be represented by Equations (18) and (19):

$$Ce^{3+} + {SO_4}^{2-} = CeSO_4^{+} \quad (18)$$

$$Ce^{3+} + 2{SO_4}^{2-} = Ce(SO_4)_2^{-} \quad (19)$$

Compared with chloride systems, the hydrolysis regions in sulfate media are considerably narrower due to the stabilization of dissolved sulfate species. Under acidic conditions, cerium remains predominantly in dissolved form, while increasing the oxidation potential promotes the stabilization of oxidized cerium compounds. Only limited stability regions corresponding to hydrolyzed species and hydroxide phases are observed within the investigated pH range.

Sulfate complexation suppresses hydrolysis reactions and stabilizes dissolved cerium species even under moderately acidic conditions. Such behavior may positively influence the leaching efficiency because dissolved rare earth species remain stable during acidic processing conditions, and premature precipitation is less likely to occur. At the same time, strong sulfate complexation may complicate subsequent purification and separation operations due to the stabilization of dissolved species in solution.

At 80 °C, a partial modification of sulfate stability regions is observed together with changes in the hydrolysis boundaries. The onset of hydrolysis is shifted from approximately pH 5 at 25 °C to pH 3.5 at 80 °C, while the transition from hydrolyzed $CeO^+$ species to $Ce(OH)_3$ occurs at approximately pH 7.5 instead of pH 8.2. Despite these shifts, the sulfate-containing phase remains thermodynamically stable over a broad pH range at both temperatures. Elevated temperature therefore modifies the equilibrium relationships between dissolved and hydrolyzed species while maintaining the strong stabilizing effect of sulfate species, which corresponds well with the enhanced dissolution efficiency commonly observed during sulfuric acid leaching performed at elevated temperatures.

### *3.6. Thermodynamic Study of the La–S–$H_2O$ System*

In sulfate systems, lanthanum stability is controlled mainly by sulfate complexation and the pH-dependent hydrolysis reactions. Since lanthanum occurs exclusively in the trivalent oxidation state, the oxidation-reduction potential has a considerably smaller

influence on the species stability than in cerium systems. The calculated stability fields for the La–S–$H_2O$ system at 25 °C and 80 °C are presented in Figure 9.

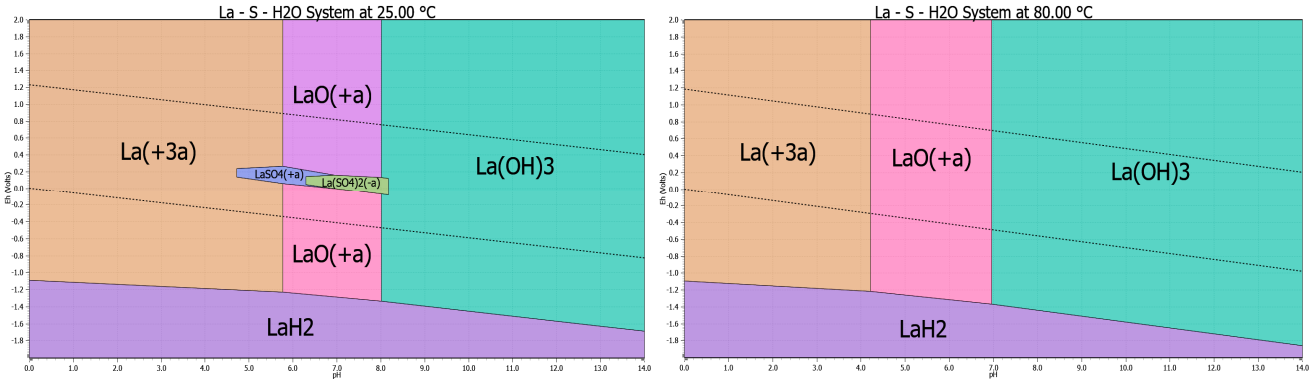


(**a**) (**b**)

**Figure 9.** Eh–pH diagrams of La leaching in $H_2SO_4$ at temperatures of 25 °C and 80 °C: (**a**) The La-S-$H_2O$ system at temperature of 25 °C; (**b**) The La-S-$H_2O$ system at temperature of 80 °C. Note: The molalities of the elements are set at 1 mol·kg$^{-1}$ $H_2O$, with the upper and lower stability limits of $H_2O$ defined by the dashed lines.

Under strongly acidic conditions, dissolved $La^{3+}$ ions together with sulfate-containing species such as $LaSO_4^+$ remain thermodynamically stable. The formation of lanthanum sulfate complexes can be expressed by Equations (20) and (21):

$$La^{3+} + SO_4^{2-} = LaSO_4^+ \quad (20)$$

$$La^{3+} + 2SO_4^{2-} = La(SO_4)_2^- \quad (21)$$

Sulfate complexation significantly stabilizes dissolved lanthanum species and suppresses hydrolysis reactions compared with chloride systems. Consequently, the precipitation of $La(OH)_3$ occurs only at higher pH values.

A gradual increase in pH promotes the formation of $LaO^+$ species, followed by hydroxide precipitation in alkaline environments. Compared with chloride media, the transition between dissolved and precipitated species occurs within narrower equilibrium regions, indicating stronger stabilization of dissolved species in sulfate systems.

At an elevated temperature, a partial simplification of the stability fields is observed, together with a reduction in the sulfate complex regions. The stability fields of sulfate-containing species, such as $LaSO_4^+$ and $La(SO_4)_2^-$, become considerably smaller at 80 °C, while the onset of hydrolysis shifts from approximately pH 6 at 25 °C to pH 4.5 at 80 °C. In addition, the precipitation of $La(OH)_3$ occurs at approximately pH 7 instead of pH 8. These changes suggest that temperature modifies sulfate complex stability and the equilibrium relationships in sulfuric acid systems while promoting hydrolysis reactions. Nevertheless, dissolved lanthanum species predominate throughout acidic conditions relevant to hydrometallurgical leaching processes.

### *3.7. Thermodynamic Study of the Nd–S–$H_2O$ System*

The predominance diagrams calculated for the Nd–S–$H_2O$ system (Figure 10) demonstrate that sulfate ions considerably influence neodymium speciation in aqueous solutions. In contrast to cerium, whose equilibrium is affected by changes in the oxidation state, neodymium remains exclusively trivalent throughout the investigated Eh–pH range. Consequently, the distribution of neodymium species is controlled mainly by sulfate complex formation and subsequent hydrolysis.

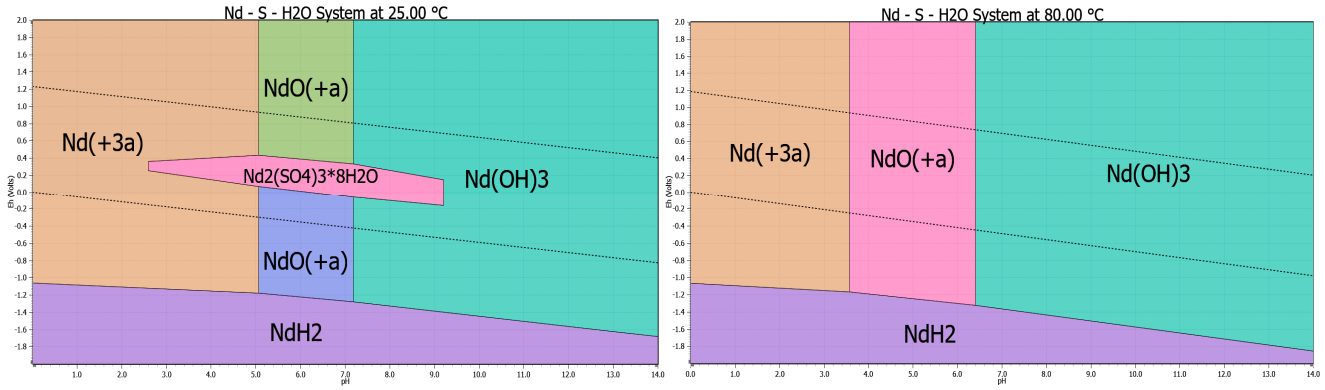


(**a**) (**b**)

**Figure 10.** Eh–pH diagrams of leaching Nd in $H_2SO_4$ at temperatures of 25 °C and 80 °C: (**a**) The Nd-S-$H_2O$ system at temperature of 25 °C; (**b**) The Nd-S-$H_2O$ system at temperature of 80 °C. Note: The molalities of the elements are set at 1mol·kg$^{-1}$ $H_2O$, with the upper and lower stability limits of $H_2O$ defined by the dashed lines.

The stabilization of dissolved neodymium species in sulfate media results from the formation of aqueous sulfate complexes, which may be described by Equations (22) and (23):

$$Nd^{+} + SO_4^{2-} = NdSO_4^{+} \quad (22)$$

$$Nd^{+} + 2SO_4^{2-} = Nd(SO_4)_2^{-} \quad (23)$$

At 25 °C, dissolved $Nd^{3+}$ species dominate under acidic conditions before gradually transforming into $NdO^{+}$ with increasing pH. Further alkalization results in the formation of $Nd(OH)_3$, which becomes the thermodynamically preferred phase above approximately pH 7. Unlike the chloride system, the sulfate diagram predicts a distinct stability field corresponding to the hydrated neodymium sulfate, $Nd_2(SO_4)_3{\cdot}8H_2O$. This phase occupies only a limited region of the diagram, suggesting that its formation is restricted to relatively narrow equilibrium conditions where the sulfate activity remains sufficiently high.

The phase relationships change noticeably at 80 °C. The hydrated sulfate phase is no longer predicted to be stable, indicating that increasing the temperature disfavors its formation. Simultaneously, the onset of hydrolysis shifts towards more acidic conditions, with $NdO^{+}$ appearing at approximately pH 4 instead of pH 5, while the precipitation of $Nd(OH)_3$ begins near pH 6, compared with approximately pH 7 at 25 °C. These shifts indicate that elevated temperature promotes hydrolysis while reducing the stability of hydrated sulfate compounds.

The calculated equilibria therefore suggest that sulfuric acid leaching performed at higher temperatures should favor the persistence of dissolved neodymium species without the formation of secondary hydrated sulfate phases. Such behavior is advantageous for hydrometallurgical processing because it minimizes the risk of intermediate sulfate precipitation while maintaining conditions suitable for the subsequent separation and recovery of neodymium from solution.

### *3.8. Thermodynamic Study of Bastnaesite and Monazite Leaching in Sulfuric Acid Media*

Sulfuric acid is widely employed in the industrial processing of bastnäsite and monazite because it facilitates the formation of soluble rare earth sulfates while suppressing hydrolysis under acidic conditions. To evaluate the thermodynamic feasibility of representative dissolution reactions, the reactions described by Equations (24)–(29) were assessed by calculating the corresponding thermodynamic parameters. The calculated enthalpy

(ΔH), entropy (ΔS), and Gibbs free energy (ΔG) values for the sulfuric acid system are summarized in Table 6.

**Table 6.** Calculated thermodynamic parameters for representative dissolution reactions of bastnäsite and monazite in sulfuric acid.

| Mineral | Chemical Reaction | T [°C] | ΔH [kJ] | ΔS [J/K] | ΔG [kJ] | No. |
|---|---|---|---|---|---|---|
| Bastnaesite | $Ce_2O_3 + 3H_2SO_{4(ia)} = Ce_2(SO_4)_{3(a)} + 3H_2O$ | 25 | −451.499 | −364.462 | −342.835 | (24) |
| | | 80 | −397.859 | −199.695 | −327.337 | |
| | $La_2O_3 + 3H_2SO_{4(ia)} = La_2(SO_4)_{3(a)} + 3H_2O$ | 25 | −534.682 | −295.723 | −446.512 | (25) |
| | | 80 | −462.106 | −72.800 | −436.396 | |
| | $CeO_2 + 2H_2SO_{4(ia)} = Ce(SO_4)_{2(a)} + 2H_2O$ | 25 | −5.473 | 239.102 | −76.762 | (26) |
| | | 80 | 31.180 | 351.699 | −93.022 | |
| Monazit | $2CePO_4 + 3H_2SO_{4(ia)} = Ce_2(SO_4)_{3(a)} + H_3PO_{4(a)}$ | 25 | −31.330 | −81.651 | −6.986 | (27) |
| | | 80 | −19.185 | −44.368 | −3.517 | |
| | $2LaPO_4 + 3H_2SO_{4(ia)} = La_2(SO_4)_{3(a)} + H_3PO_{4(a)}$ | 25 | −162.033 | −270.889 | −81.267 | (28) |
| | | 80 | −92.266 | −56.692 | −72.246 | |
| | $2NdPO_4 + 3H_2SO_{4(ia)} = La_2(SO_4)_{3(a)} + H_3PO_{4(a)}$ | 25 | 234.638 | 300.792 | 144.956 | (29) |
| | | 80 | 300.846 | 504.151 | 122.805 | |

Note: (a) denotes an aqueous species, while (ia) denotes an ion-associated aqueous species according to the HSC Chemistry database notation.

In sulfuric acid media, cerium stability is strongly influenced by sulfate complexation and the formation of sulfate-bearing phases. The calculated Eh–pH diagrams for the Ce–S–F–C–$H_2O$ system at 25 °C and 80 °C are presented in Figure 11. The sulfate species occupy an extensive stability region, indicating a strong interaction between cerium and sulfate ions under acidic conditions. This behavior is consistent with previous studies showing that sulfuric acid leaching and baking are effective routes for converting rare-earth-bearing phases into sulfate species during bastnäsite processing.

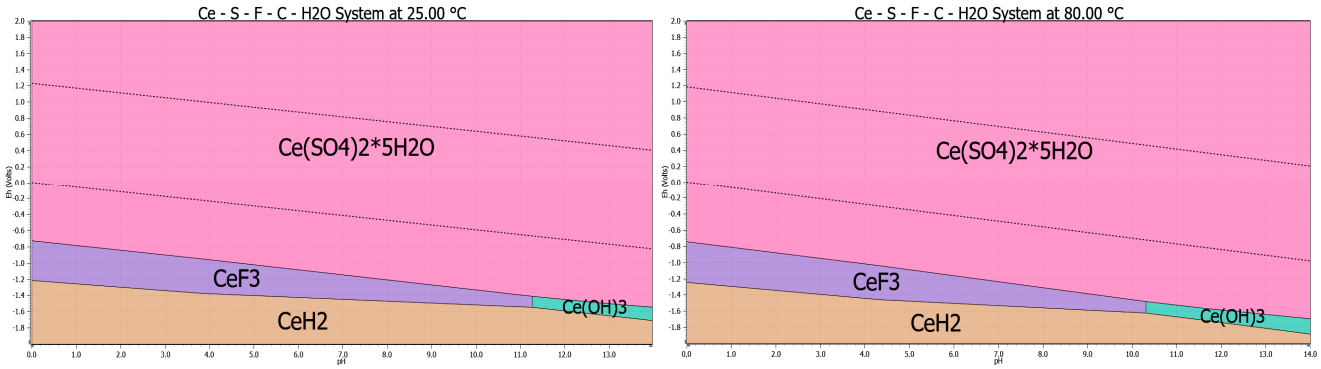


(**a**) (**b**)

**Figure 11.** Eh–pH diagrams of leaching bastnaesite in $H_2SO_4$ at temperatures of 25 °C and 80 °C: (**a**) The Ce-F-C-S-$H_2O$ system at temperature of 25 °C; (**b**) The Ce-F-C-S-$H_2O$ system at temperature of 80 °C. Note: The molalities of the elements are set at 1 mol·kg$^{-1}$ $H_2O$, with the upper and lower stability limits of $H_2O$ defined by the dashed lines.

The Eh–pH diagrams show that the tetravalent cerium sulfate hydrate, $Ce(SO_4)_2 \cdot 5H_2O$, is stable over a wide oxidizing region. This indicates that sulfate media strongly stabilize cerium in sulfate-bearing forms. Compared with hydrochloric acid systems, the stability field of $CeO_2$ is not dominant in the investigated sulfuric acid system; instead, sulfate-bearing cerium phases prevail.

Increasing the temperature from 25 °C to 80 °C does not fundamentally change the dominant stability field of $Ce(SO_4)_2 \cdot 5H_2O$. Only slight shifts in the stability boundaries of $CeF_3$, $CeH_2$ and $Ce(OH)_3$ are observed. These results indicate that sulfate complexation controls cerium speciation in sulfuric acid media and suppresses extensive hydrolysis over a broad pH range.

Figure 12 illustrates the variation in Gibbs free energy with temperature for the representative dissolution reactions of $Ce_2O_3$, $La_2O_3$ and $CeO_2$ in sulfuric acid. The figure enables a direct comparison of the thermodynamic behavior of trivalent and tetravalent rare earth oxides over a broad temperature interval.

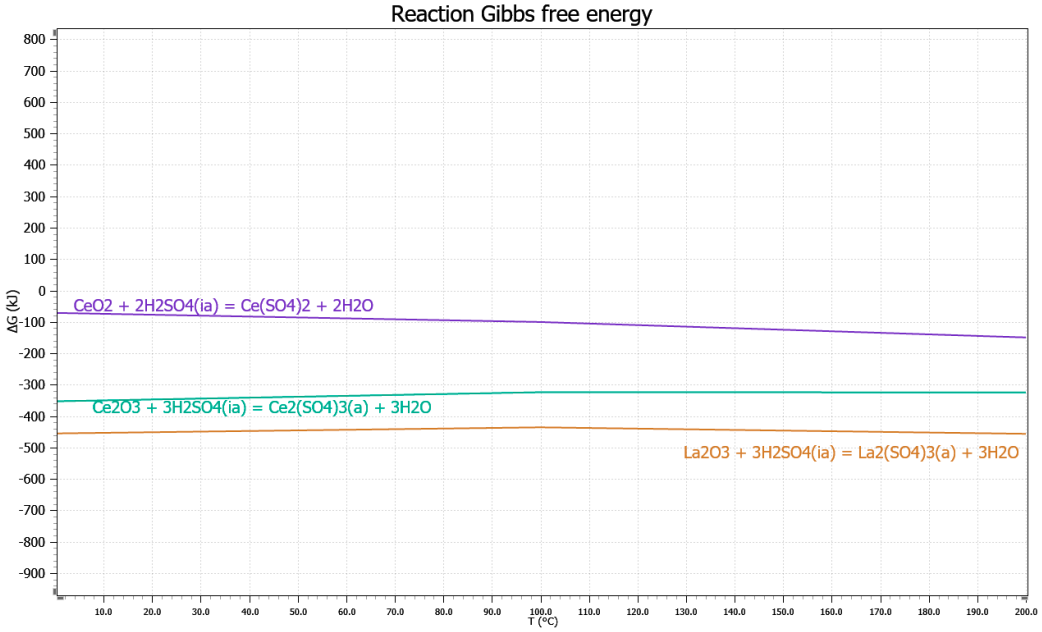


**Figure 12.** Graph of dependence of ΔG values of Equations (24)–(26) on temperature. Note: "a" denotes an aqueous species, while "ia" denotes an ion-associated aqueous species according to the HSC Chemistry database notation.

As shown in Figure 10, the dissolution of $Ce_2O_3$ and $La_2O_3$ remains thermodynamically favorable throughout the investigated temperature range, as indicated by the negative Gibbs free energy values. In contrast to hydrochloric acid, the dissolution of tetravalent cerium also becomes thermodynamically more favorable due to the stabilization of sulfate species. The relatively small variation in ΔG with temperature indicates that sulfate complexation exerts a considerably stronger influence on reaction spontaneity than temperature alone.

Overall, the thermodynamic analysis demonstrates that sulfuric acid efficiently stabilizes dissolved rare earth sulfates and suppresses hydrolysis over a broad acidic pH range. These characteristics explain the widespread industrial application of sulfuric acid in bastnäsite processing.

Sulfuric acid is widely employed industrially because it gradually converts rare earth phosphates into soluble sulfate species. Representative dissolution reactions of $CePO_4$, $LaPO_4$ and $NdPO_4$ in sulfuric acid were therefore evaluated to assess the thermodynamic feasibility of phosphate decomposition.

The calculated thermodynamic parameters are summarized in Table 6, while Figure 13 illustrates the variation in the Gibbs free energy with temperature for the representative dissolution reactions of monazite in sulfuric acid.

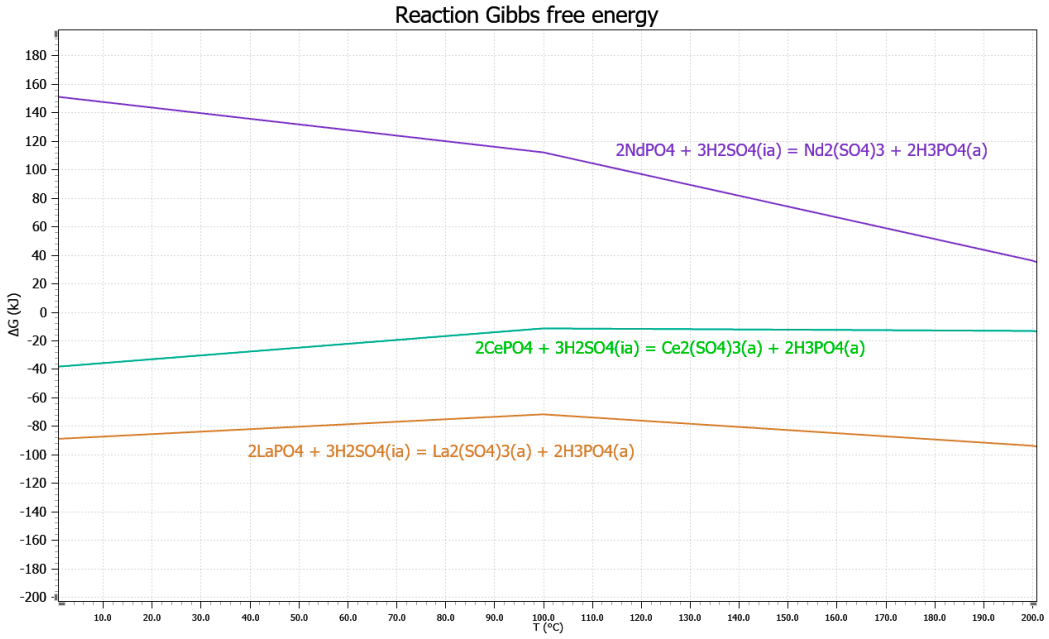


**Figure 13.** Graph of dependence of ΔG values of Equations (27)–(29) on temperature. Note: "a" denotes an aqueous species, while "ia" denotes an ion-associated aqueous species according to the HSC Chemistry database notation.

As shown in Figure 13, all investigated phosphate minerals exhibit similar thermodynamic behavior over the investigated temperature range. The Gibbs free energy values decrease progressively with increasing the temperature, indicating that elevated temperatures improve the thermodynamic feasibility of the phosphate dissolution. Nevertheless, the phosphate lattice remains considerably more stable than the corresponding oxide phases derived from bastnäsite, reflecting the high stability of the REE–phosphate bonds.

Among the investigated phosphates, only minor differences are observed. Cerium and lanthanum phosphates exhibit nearly identical thermodynamic behavior, whereas neodymium phosphate remains slightly more stable, as indicated by its consistently higher Gibbs free energy values.

Although elevated temperatures improve the thermodynamic driving force of the phosphate dissolution, practical monazite processing still requires aggressive leaching conditions because of the exceptional stability of the phosphate structure. Consequently, industrial sulfuric acid processing frequently employs concentrated sulfuric acid together with elevated temperatures during the acid baking to enhance the decomposition of monazite and the subsequent formation of soluble rare earth sulfates.

Overall, the comparison of bastnäsite and monazite demonstrates that sulfuric acid promotes sulfate formation in both minerals; however, the dissolution of monazite remains thermodynamically less favorable owing to the greater stability of the phosphate lattice. These findings confirm that the mineralogical composition, together with the sulfate complexation, plays a decisive role in determining the thermodynamic feasibility of rare earth leaching and provides valuable guidance for the optimization of industrial hydrometallurgical processes.

### *3.9. Comparison of Chloride and Sulfate Systems*

The comparison of chloride and sulfate systems demonstrated substantial differences in the stability of dissolved and solid REE species. Although acidic conditions favored the dissolution of rare earth elements in both media, differences were observed in the extent of hydrolysis, aqueous complex formation and precipitation behavior.

In chloride systems, dissolved REE species remained stable predominantly under strongly acidic conditions. Increasing the pH promoted hydrolysis reactions, leading to the formation of hydrolyzed species and the subsequent precipitation of hydroxides. The relatively limited complexation in chloride media resulted in more distinct stability boundaries between dissolved and solid phases.

In contrast, sulfate systems exhibited broader stability regions of dissolved REE species. This behavior can be attributed to the formation of sulfate-containing aqueous complexes, which increased the stability of dissolved species and suppressed hydrolysis reactions. Consequently, the precipitation regions were generally less extensive than those observed in the corresponding chloride systems.

Temperature affected both systems by causing moderate shifts in the equilibrium boundaries and hydrolysis regions. However, the overall thermodynamic trends remained unchanged. The obtained results suggest that sulfate media provide more favorable conditions for maintaining REEs in a dissolved form during leaching, whereas chloride systems exhibit more distinct precipitation boundaries that may be advantageous during the subsequent recovery and purification stages.

A comparison of the principal characteristics of chloride and sulfate systems is presented in Table 7.

**Table 7.** Comparison of the thermodynamic behavior of REEs[1] in chloride and sulfate systems.

| Parameter | Chloride System | Sulfate System |
|---|---|---|
| Dominant dissolved species in acidic media | $Ce^{3+}$, $La^{3+}$, $Nd^{3+}$, $LaCl^{2+}$, $NdCl^{2+}$ | $Ce^{3+}$, $La^{3+}$, $Nd^{3+}$, $LaSO_4^{+}$, $La(SO_4)_2^{-}$, $NdSO_4^{+}$, $Nd(SO_4)_2^{-}$ |
| Stability of dissolved REE [1] species | Stable mainly under strongly acidic conditions (typically below pH 5–6) | Stable over a broader acidic pH range due to sulfate complexation |
| Complexation behavior | Limited chloride complexation | Strong sulfate complexation |
| Hydrolysis tendency | More pronounced with increasing pH | Suppressed by sulfate complexation |
| Onset of hydrolysis | Ce: pH ≈ 5 (25 °C), pH ≈ 4 (80 °C); La: pH ≈ 6 (25 °C), pH ≈ 4.5 (80 °C); Nd: pH ≈ 5 (25 °C), pH 4 (80 °C) | Ce: pH ≈ 5 (25 °C), pH ≈ 4 (80 °C); La: pH ≈ 6 (25 °C), pH ≈ 4.5 (80 °C); Nd: pH ≈ 5 (25 °C), pH 4 (80 °C) |
| Onset of hydroxide precipitation | $Ce(OH)_3$: pH ≈ 8.5 (25 °C), pH ≈ 7.5 (80 °C); $La(OH)_3$: pH ≈ 8.0 (25 °C), pH ≈ 7.0 (80 °C); $Nd(OH)_3$: pH ≈ 7.2 (25 °C), pH ≈ 6.4 (80 °C) | $Ce(OH)_3$: pH ≈ 8.5 (25 °C), pH ≈ 7.5 (80 °C); $La(OH)_3$: pH ≈ 8.0 (25 °C), pH ≈ 7.0 (80 °C); $La(OH)_3$: pH ≈ 7.0 (25 °C), pH ≈ 6.0 (80 °C) |
| Stability of dissolved species | Lower at moderately acidic pH values | Higher due to sulfate complex formation |
| Effect of temperature | Shifts hydrolysis and precipitation boundaries toward lower pH values | Similar shifts toward lower pH values accompanied by modification of sulfate complex stability |
| Implications for leaching | Favorable under strongly acidic conditions | Enhanced stability of dissolved REEs[1] during leaching |

[1] REE, Rare earth element.

## 4. Conclusions

This study evaluated the aqueous stability of cerium and lanthanum in chloride and sulfate media using Eh–pH diagrams generated in the HSC Chemistry software. The obtained results confirmed that physicochemical conditions strongly influence the dissolution and precipitation behavior of rare earth species during hydrometallurgical processing.

Both the hydrochloric and sulfuric acid systems provided favorable conditions for the dissolution of rare earth elements in strongly acidic environments. Nevertheless, significant differences were observed between the chloride and sulfate media. Chloride systems were characterized by simpler aqueous chemistry and wider hydrolysis regions, whereas sulfate systems promoted stronger complexation effects and the stabilization of dissolved

species over broader acidic intervals. Sulfate complexation simultaneously suppressed hydrolysis reactions and modified the equilibrium relationships between the dissolved and precipitated phases.

The comparison of the cerium and lanthanum systems highlighted the importance of cerium redox behavior in hydrometallurgical environments. While lanthanum remained stable exclusively in the trivalent oxidation state, cerium exhibited more complex equilibrium relationships associated with the oxidation of $Ce^{3+}$ to $Ce^{4+}$ and the stabilization of $CeO_2$ under oxidizing conditions. Such behavior may be advantageous during the selective separation of cerium from other trivalent rare earth elements in downstream purification processes.

Increasing the temperature from 25 °C to 80 °C caused moderate shifts in the equilibrium boundaries together with a partial modification of the hydrolysis and sulfate complex regions. Elevated temperature generally promotes the stabilization of dissolved species, which corresponds well with the enhanced dissolution efficiency commonly observed during hydrometallurgical leaching at elevated temperatures.

The performed thermodynamic analysis confirmed that Eh–pH diagrams represent valuable tools for the prediction of equilibrium conditions in rare earth leaching systems and for the evaluation of factors influencing the dissolution, hydrolysis and precipitation of REE species. The obtained results may support the further optimization of the hydrometallurgical processes used for rare earth element extraction and separation.

Building upon these findings, future research should focus on the experimental validation of the calculated Eh–pH diagrams using laboratory leaching tests. Thermodynamic studies represent an important preliminary step in the development of hydrometallurgical processes, as they provide valuable information regarding species stability, favorable leaching conditions and potential dissolution–precipitation behavior under different process parameters. Such knowledge can significantly reduce the number of experimental trials required during process development and facilitate the selection of suitable leaching systems.

The next stage of this research will involve the application of the obtained thermodynamic results to the laboratory-scale experiments using REE-bearing raw materials. Particular attention will be devoted to evaluating the agreement between the predicted equilibrium conditions and the experimentally observed leaching behavior. Furthermore, the presented methodology can be extended to additional REEs and more complex aqueous systems relevant to industrial hydrometallurgical processing. The integration of thermodynamic modeling with experimental investigations may contribute to the development of more efficient, selective and sustainable technologies for the recovery of REEs from primary and secondary resources.

**Author Contributions:** Conceptualization, E.G. and M.L.; methodology, E.G. and M.S.; software, J.K.; validation, M.L. and M.S.; formal analysis, E.G. and M.L.; investigation, E.G. and M.L.; resources, E.G. and M.S.; data curation, E.G. and M.L.; writing—original draft preparation, E.G.; writing—review and editing, M.L.; visualization, J.K. and E.G.; supervision, M.L. and M.S.; project administration, E.G. All authors have read and agreed to the published version of the manuscript.

**Funding:** Funded by the EU NextGenerationEU through the Recovery and Resilience Plan for Slovakia under project No. 09I03-03-V05-00015. This work was supported by the Slovak Cultural and Educational Grant Agency under the grant project KEGA 023TUKE-4/2026 "Innovation of the profile subjects of the new study program "Environmental Protection and Ecotechnologies of Raw Materials" in accordance with the requirements of professional practice."

**Data Availability Statement:** The original contributions presented in the study are included in the article. Further inquiries can be directed to the corresponding author.

**Conflicts of Interest:** The authors declare no conflicts of interest.

## References


1. Gajendra, N.; Yilmaz, D.; Vila, M.C.; de Lurdes Dinis, M.; Levei, E.; Merrild, A.; Ferrando-Climent, L. Towards a European sustainable beneficiation of rare earth elements bearing minerals. *Sci. Total Environ.* **2025**, *980*, 179386. [CrossRef] [PubMed]
2. Wang, Z.Y.; Fan, H.R.; Zhou, L.; Yang, K.F.; She, H.D. Carbonatite-related REE deposits: An overview. *Minerals* **2020**, *10*, 965. [CrossRef]
3. *European Commission, Study on the Critical Raw Materials for the EU 2023—Final Report*; Publications Office of the European Union: Luxembourg, 2023.
4. Chen, P.; Ilton, E.S.; Wang, Z.; Rosso, K.M.; Zhang, X. Global rare earth element resources: A concise review. *Appl. Geochem.* **2024**, *175*, 106158. [CrossRef]
5. Kanazawa, Y.; Kamitani, M. Rare earth minerals and resources in the world. *J. Alloys Compd.* **2006**, *408*, 1339–1343. [CrossRef]
6. Rezaei, M.; Sanchez-Lecuona, G.; Abdolazimi, O. A cross-disciplinary review of rare earth elements: Deposit types, mineralogy, machine learning, environmental impact, and recycling. *Minerals* **2025**, *15*, 720. [CrossRef]
7. Julapong, P.; Numprasanthai, A.; Tangwattananukul, L.; Juntarasakul, O.; Srichonphaisarn, P.; Aikawa, K.; Phengsaart, T. Rare earth elements recovery from primary and secondary resources using flotation: A systematic review. *Appl. Sci.* **2023**, *13*, 8364. [CrossRef]
8. Cheng, S.; Li, W.; Han, Y.; Sun, Y.; Gao, P.; Zhang, X. Recent process developments in beneficiation and metallurgy of rare earths: A review. *J. Rare Earths* **2024**, *42*, 629–642.
9. Shahbaz, A. A systematic review on leaching of rare earth metals from primary and secondary sources. *Miner. Eng.* **2022**, *184*, 107632. [CrossRef]
10. Lin, P.; Yang, X.; Werner, J.M.; Honaker, R.Q. Application of Eh-pH diagrams on acid leaching systems for the recovery of REEs from bastnaesite, monazite and xenotime. *Metals* **2021**, *11*, 734.
11. Kim, E.; Osseo-Asare, K. Aqueous stability of thorium and rare earth metals in monazite hydrometallurgy: Eh–pH diagrams for the systems Th–, Ce–, La–, Nd–($PO_4$)–($SO_4$)–$H_2O$ at 25 C. *Hydrometallurgy* **2012**, *113*, 67–78.
12. Shuai, Z.; Zhu, Y.; Gao, P.; Han, Y. Rare earth elements resources and beneficiation: A review. *Miner. Eng.* **2024**, *218*, 109011. [CrossRef]
13. Balaram, V. Rare earth element deposits: Sources, and exploration strategies. *J. Geol. Soc. India* **2022**, *98*, 1210–1216. [CrossRef]
14. Beland, C.M.; Williams-Jones, A.E. The mineralogical distribution of the REE in carbonatites: A quantitative evaluation. *Chem. Geol.* **2021**, *585*, 120558. [CrossRef]
15. Liu, S.L.; Fan, H.R.; Liu, X.; Meng, J.; Butcher, A.R.; Yann, L.; Li, X.C. Global rare earth elements projects: New developments and supply chains. *Ore Geol. Rev.* **2023**, *157*, 105428. [CrossRef]
16. Dostal, J. Rare earth element deposits of alkaline igneous rocks. *Resources* **2017**, *6*, 34. [CrossRef]
17. Negash, B.M.; Effiong, A.J.; Khan, H.W.; Zulkifli, N.I. Ion-adsorbed REE clays: Swelling challenges and future solutions. *J. Mol. Liq.* **2024**, *403*, 124849. [CrossRef]
18. Balaram, V. Rare earth elements: A review of applications, occurrence, exploration, analysis, recycling, and environmental impact. *Geosci. Front.* **2019**, *10*, 1285–1303. [CrossRef]
19. *ISO 22444-1:2020*; Rare earth—Vocabulary—Part 1: Minerals, Oxides and Other Compounds. ISO: Geneva, Switzerland, 2020.
20. Jha, M.K.; Kumari, A.; Panda, R.; Kumar, J.R.; Yoo, K.; Lee, J.Y. Review on hydrometallurgical recovery of rare earth metals. *Hydrometallurgy* **2016**, *165*, 2–26. [CrossRef]
21. Jordens, A.; Cheng, Y.P.; Waters, K.E. A review of the beneficiation of rare earth element bearing minerals. *Miner. Eng.* **2013**, *41*, 97–114. [CrossRef]
22. Zheng, Q.; Xu, Y.; Cui, L.; Ma, S.; Guan, W. Nonoxidative microwave radiation roasting of bastnasite concentrate and kinetics of hydrochloric acid leaching process. *ACS Omega* **2020**, *5*, 26710–26719. [CrossRef] [PubMed]
23. Demol, J.; Ho, E.; Senanayake, G. Sulfuric acid baking and leaching of rare earth elements, thorium and phosphate from a monazite concentrate: Effect of bake temperature from 200 to 800 C. *Hydrometallurgy* **2018**, *179*, 254–267. [CrossRef]
24. Li, S.; Malik, M.; Azimi, G. Extraction of rare earth elements from phosphogypsum using mineral acids: Process development and mechanistic investigation. *Ind. Eng. Chem. Res.* **2021**, *61*, 102–114. [CrossRef]
25. Zhang, D.; Li, M.; Gao, K.; Li, J.; Yan, Y.; Liu, X. Physical and chemical mechanism underlying ultrasonically enhanced hydrochloric acid leaching of non-oxidative roasting of bastnaesite. *Ultrason. Sonochem.* **2017**, *39*, 774–781. [CrossRef]
26. Moldoveanu, G.A.; Papangelakis, V.G. Recovery of rare earth elements adsorbed on clay minerals: II. Leaching with ammonium sulfate. *Hydrometallurgy* **2013**, *131*, 158–166. [CrossRef]
27. Battsengel, A.; Batnasan, A.; Narankhuu, A.; Haga, K.; Watanabe, Y.; Shibayama, A. Recovery of light and heavy rare earth elements from apatite ore using sulphuric acid leaching, solvent extraction and precipitation. *Hydrometallurgy* **2018**, *179*, 100–109. [CrossRef]
28. Huang, X.W.; Long, Z.Q.; Wang, L.S.; Feng, Z.Y. Technology development for rare earth cleaner hydrometallurgy in China. *Rare Met.* **2015**, *34*, 215–222. [CrossRef]

29. Gupta, C.K.; Krishnamurthy, N. Extractive metallurgy of rare earths. *Int. Mater. Rev.* **1992**, *37*, 197–248. [CrossRef]
30. Xie, F.; Zhang, T.A.; Dreisinger, D.; Doyle, F. A critical review on solvent extraction of rare earths from aqueous solutions. *Miner. Eng.* **2014**, *56*, 10–28. [CrossRef]
31. Peelman, S.; Sun, Z.H.I.; Sietsma, J.; Yang, Y. Leaching of rare earth elements: Past and present. In Proceedings of the ERES2014: First European Rare Earth Resources Conference, Milos, Greece, 4–6 September 2014.
32. Zhang, X.W.; Li, M.; Liu, Z.G.; Hu, Y.H.; Wang, M.T. Kinetics of rare earth extraction from Baotou bastnaesite in hydrochloric acid and aluminum chloride. *JOM* **2017**, *69*, 1894–1900. [CrossRef]
33. Bian, X.; Yin, S.H.; Zhang, F.Y.; Wu, W.Y.; Tu, G.F. Study on leaching process of activation bastnaesite by HCl solution. *Adv. Mater. Res.* **2011**, *233*, 1406–1410. [CrossRef]
34. Feng, X.L.; Long, Z.Q.; Cui, D.L.; Wang, L.S.; Huang, X.W.; Zhang, G.C. Kinetics of rare earth leaching from roasted ore of bastnaesite with sulfuric acid. *Trans. Nonferrous Met. Soc. China* **2013**, *23*, 849–854. [CrossRef]
35. Kul, M.; Topkaya, Y.A.V.U.Z.; Karakaya, İ. Rare earth double sulfates from pre-concentrated bastnasite. *Hydrometallurgy* **2008**, *93*, 129–135. [CrossRef]
36. Yörükoğlu, A.; Obut, A.; Girgin, I. Effect of thiourea on sulphuric acid leaching of bastnaesite. *Hydrometallurgy* **2003**, *68*, 195–202. [CrossRef]
37. Chi, R.; Zhang, X.; Zhu, G.; Zhou, Z.A.; Wu, Y.; Wang, C.; Yu, F. Recovery of rare earth from bastnasite by ammonium chloride roasting with fluorine deactivation. *Miner. Eng.* **2004**, *17*, 1037–1043. [CrossRef]
38. Cen, P.; Wu, W.; Bian, X. A novel process for recovery of rare earth and fluorine from bastnaesite concentrates. Part I: Calcification roasting decomposition. *Green Process. Synth.* **2016**, *5*, 427–434. [CrossRef]
39. Zhang, Q.; Saito, F. Non-thermal process for extracting rare earths from bastnaesite by means of mechanochemical treatment. *Hydrometallurgy* **1998**, *47*, 231–241. [CrossRef]
40. He, J.; Li, Y.; Xue, X.; Ru, H.; Huang, X.; Yang, H. Leaching of fluorine and rare earths from bastnaesite calcined with aluminum hydroxide and the recovery of fluorine as cryolite. *RSC Adv.* **2017**, *7*, 14053–14059. [CrossRef]
41. Panda, R.; Kumari, A.; Jha, M.K.; Hait, J.; Kumar, V.; Kumar, J.R.; Lee, J.Y. Leaching of rare earth metals (REMs) from Korean monazite concentrate. *J. Ind. Eng. Chem.* **2014**, *20*, 2035–2042. [CrossRef]
42. Sadri, F.; Rashchi, F.; Amini, A. Hydrometallurgical digestion and leaching of Iranian monazite concentrate containing rare earth elements Th, Ce, La and Nd. *Int. J. Mineral. Process.* **2017**, *159*, 7–15. [CrossRef]
43. Sadri, F.; Nazari, A.M.; Ghahreman, A. A review on the cracking, baking and leaching processes of rare earth element concentrates. *J. Rare Earths* **2017**, *35*, 739–752. [CrossRef]
44. Moldoveanu, G.A.; Papangelakis, V.G. An overview of rare-earth recovery by ion-exchange leaching from ion-adsorption clays of various origins. *Mineral. Mag.* **2016**, *80*, 63–76.
45. Moldoveanu, G.A.; Papangelakis, V.G. Recovery of rare earth elements adsorbed on clay minerals: I. Desorption mechanism. *Hydrometallurgy* **2012**, *117*, 71–78. [CrossRef]
46. Huang, X.W.; Huang, L. Leaching characteristics of ion-adsorption type rare earths ore with magnesium sulfate. *Trans. Nonferrous Met. Soc. China* **2015**, *25*, 3784–3790. [CrossRef]
47. Han, M.; Wang, D.; Rao, Y.; Xu, W.; Nie, W. An experimental study on the kinetics of leaching ion-adsorbed REE deposits with different concentrations of magnesium sulfate. *Metals* **2023**, *13*, 1906. [CrossRef]
48. Kollová, A.; Laubertová, M.; Trpčevská, J.; Sisol, M. Thermodynamic Study of the Sustainable Hydrometallurgical Treatment of Copper Converter Flue Dust Based on Pb, Zn, and Sn Oxides. *Materials* **2024**, *17*, 5690. [CrossRef] [PubMed]
49. Pourbaix, M. *Atlas of Electrochemical Equilibria in Aqueous Solutions*, 2nd ed.; National Association of Corrosion Engineers: Houston, TX, USA, 1974.
50. Han, K.N.; Kim, R. Thermodynamic analysis of precipitation characteristics of rare earth elements with sulfate in comparison with other common precipitants. *Minerals* **2021**, *11*, 670. [CrossRef]